The Moisture Budget of Tropical Cyclones in HighResMIP Models: Large-Scale Environmental Balance and Sensitivity to Horizontal Resolution

BENOÎT VANNIÈRE,[a] MALCOLM ROBERTS,[b] PIER LUIGI VIDALE,[a] KEVIN HODGES,[a] MARIE-ESTELLE DEMORY,[c] LOUIS-PHILIPPE CARON,[d] ENRICO SCOCCIMARRO,[e] LAURENT TERRAY,[f] AND RETISH SENAN[g]

[a] *National Centre for Atmospheric Science, Department of Meteorology, University of Reading, Reading, United Kingdom*
[b] *Met Office Hadley Center, Exeter, United Kingdom*
[c] *Institute for Atmospheric and Climate Science, Department of Environmental Systems Science, ETH Zürich, Zürich, Switzerland*
[d] *Barcelona Supercomputing Center, Barcelona, Spain*
[e] *Fondazione Centro Euro-Mediterraneo sui Cambiamenti Climatici, Bologna, Italy*
[f] *Climat, Environnement, Couplages, Incertitudes, Université de Toulouse, CNRS, Cerfacs, Toulouse, France*
[g] *European Centre for Medium-Range Weather Forecasts, Reading, United Kingdom*

(Manuscript received 28 December 2019, in final form 15 May 2020)

ABSTRACT

Previous studies have shown that the number, intensity, and structure of simulated tropical cyclones (TCs) in climate models get closer to the observations as the horizontal resolution is increased. However, the sensitivity of tropical cyclone precipitation and moisture budget to changes in resolution has received less attention. In this study, we use the five-model ensemble from project PRIMAVERA/HighResMIP to investigate the systematic changes of the water budget of tropical cyclones in a range of horizontal resolutions from 1° to 0.25°. Our results show that, despite a large change in the distribution of TC intensity with resolution, the distribution of precipitation per TC (i.e., averaged in a 5° radial cap) does not change significantly. This result is explained by the fact that low- and high-resolution models represent equally well the large-scale balance that characterizes the moisture budget of TCs, with the radius of the moisture source extending to ~15° from the center of the TC (i.e. well beyond the TC edge). The wind profile is found to converge in the low and high resolutions for radii > 5°, resulting in a moisture flux convergence into the TC of similar magnitude at low and high resolutions. In contrast to precipitation per TC, TC intensity does increase at higher resolution and this is explained by the larger surface latent heat flux near the center of the storm, which leads to an increase in equivalent potential temperature and warmer core anomalies, although this extra latent heat represents a negligible contribution to the overall moisture budget. We discuss the complication arising from the choice of the tracking algorithm when assessing the impact of model resolution.

1. Introduction

Tropical cyclone precipitation (TCP) has received increasing attention over the past decade, as observational datasets of precipitation became more reliable and tropical cyclone track records more comprehensive. Collectively, tropical cyclones have a profound effect on the mean hydrological cycle: they contribute to a substantial fraction of total precipitation in the tropics, between 6% and 9% (Jiang and Zipser 2010), and up to 40% in the west Pacific (Jiang and Zipser 2010; Skok et al. 2013; Guo et al. 2017). Their influence on the global atmospheric circulation was also shown to have a drying effect in the region of the Maritime Continent (Scoccimarro et al. 2020). Individually, tropical cyclones can cause intense rainfall, which, after they make landfall, and together with storm surge, can cause coastal flooding with large societal impacts. Previous studies have estimated TCP from general circulation models (GCMs) using objective tracking algorithms to identify tropical cyclone tracks. Future climate projections

Supplemental information related to this paper is available at the Journals Online website: https://doi.org/10.1175/JCLI-D-19-0999.s1.

Corresponding author: Benoît Vannière, b.vanniere@reading.ac.uk

DOI: 10.1175/JCLI-D-19-0999.1

© 2020 American Meteorological Society. For information regarding reuse of this content and general copyright information, consult the AMS Copyright Policy (www.ametsoc.org/PUBSReuseLicenses).

Downloaded from http://journals.ametsoc.org/jcli/article-pdf/33/19/8457/4995419/jcli190999.pdf by guest on 16 September 2020

derived from GCMs indicate that TCP will increase at a rate predicted by the Clausius–Clapeyron relation of ~7% K^{-1} or greater (Knutson et al. 2010; Villarini and Vecchi 2012; Scoccimarro et al. 2014; Bacmeister et al. 2016).

The impact of the horizontal resolution on TC characteristics is now well documented (Caron et al. 2011; Manganello et al. 2012; Strachan et al. 2013; Roberts et al. 2015; Shaevitz et al. 2014; Bacmeister et al. 2014; Roberts et al. 2020): when compared to observations from the global references for tropical cyclones tracks IBTrACS (International Best Track Archive for Climate Stewardship; https://www.ncdc.noaa.gov/ibtracs/), increasing horizontal resolution leads to an annual count of TCs closer to the observations, both globally and per ocean basin, a more realistic spatial distribution of TCs, and a larger number of TCs of strong intensity. In addition, GCMs, which tend to underestimate maximum 10-m wind for a given minimum sea level pressure, simulate a relationship between those two quantities that converges toward IBTrACS when resolution increases. All these improvements come from an increase of TC seeds at higher resolution, a better representation of pressure gradients in the core region, a finer representation of processes leading to TC intensification, in particular moist processes, or, in some cases, an improvement of the large-scale environmental conditions. However, while some models simulate a number of tropical cyclones per year in close agreement with the observations when their grid spacing comes close to 0.25°, their intensity still remains underestimated at these resolutions. It is less clear however, how resolution affects the moisture budget of tropical cyclones and thereby their contribution to the global hydrological cycle. In this study, we will assess the reliability of the moisture budget of TCs in GCMs and the potential for improvement when horizontal resolution is increased in the range of 1°–0.25°.

We have several reasons to believe that increasing the resolution of atmospheric GCMs (AGCMs) will change the moisture budget of tropical cyclones. The complex nature of scale interactions, in particular the role of convective processes in the mesoscale range, has long been recognized to play a crucial role for tropical cyclone intensification (Ooyama 1982; Simpson et al. 1997). When resolution is increased, some mesoscale features start to become better represented, such as rainbands wrapping around the core of tropical cyclones (Manganello et al. 2012). For instance, Manganello et al. (2012) showed in a 10-km resolution model that the contraction and broadening of rainbands is associated with fluctuations of the intensity of TCs. Note that we expect further improvements for resolutions beyond the range investigated in this study. It has been shown for instance that when resolution is increased across convective scales (in the range from 8 to 1 km), usually in limited-area models, a broader range of downdrafts and updrafts is simulated with an impact on precipitation (Gentry and Lackmann 2010). Moreover, hot towers, which play an important role in precipitation efficiency (Montgomery et al. 2006), have a scale of ~5 km, which is finer than the highest resolution of the High Resolution Model Intercomparison Project (HighResMIP) ensemble.

On the other hand, the impact of resolution on the moisture budget of tropical cyclones might be limited if it is controlled by large-scale environmental parameters that low-resolution models can capture. In the tropics and in the outer region of tropical cyclones, the Rossby radius of deformation (Ro) has typical values of 1000 km and the domain over which tropical cyclones exert their influence extends farther than the core region, in cyclostrophic balance. Around 80% of the precipitation occurring within 400 km from the center of the storm is balanced by the convergence of moisture fluxes at 400 km (Braun 2006; Trenberth et al. 2007). Trenberth et al. (2007) empirically estimated the moisture source of tropical cyclones and found that this can be as far as 1600 km from the center of the storm.

As the gray zone is entered, in which convective processes start to be resolved by climate models, some uncertainty might arise from the dependency of physical parameterizations on model resolution, in particular for parameterizations directly involved in the development of tropical cyclones (i.e., convection, surface drag, and boundary layer physics) (Smith 2000; Reed and Jablonowski 2011; Zhao et al. 2012). When comparing three configurations of two GCMs at a resolution of 50 km, Kim et al. (2018) showed that the model simulating the most intense storms had, respectively, the largest precipitation rates near the core (resulting in more concentrated diabatic heating), the greatest contrast in relative humidity and surface latent heat flux between the inner and outer regions of TCs, and the greatest moisture sensitivity to convection. These results show the importance of feedbacks between surface evaporation and convection for TC intensification, and the authors attributed different feedback values to differences in convection schemes. Knutson and Tuleya (2004) found that the fractional change of precipitation averaged over a 1° cap in response to global warming was more sensitive to the choice of the parameterization of convection than the fractional change of intensity. In contrast, Patricola and Wehner (2018) compared projections of TCP in an ensemble of simulations going from a resolution of 27 km with parameterized convection to 3 km with explicit convection. They stated that the convective parameterization introduced minimal

Downloaded from http://journals.ametsoc.org/jcli/article-pdf/33/19/8457/4995419/jcli190099.pdf by guest on 16 September 2020

uncertainty into the sign of projected changes in tropical cyclone intensity and rainfall, which allowed them to have "confidence in projections from global models with parameterized convection and resolutions fine enough to include tropical cyclones" (p. 339).

A couple of recent studies have shown the value of a process-oriented evaluation of GCMs in a multimodel framework to address the role of dynamical cores and parameterizations in the representation of TCs (Kim et al. 2018; Moon et al. 2020; Wing et al. 2019). However, those studies are based on an ensemble of opportunity, formed of simulations that do not follow a single protocol, making the model comparison sometimes difficult. In addition, this ensemble is mostly made of simulations with horizontal resolution higher than 50 km and the sensitivity to resolution could not be fully addressed.

To understand the biases of tropical cyclone precipitation in GCMs, evaluate the frequency of extreme precipitation, and estimate the confidence in projected changes of TCP in a warmer climate, a better understanding of the physical mechanisms controlling the moisture budget of TCs in GCMs and in present climate is required. This study will investigate whether the moisture budget of tropical cyclones in models is sensitive to their horizontal resolution or whether it is constrained by the large-scale environment. To do so, we will use a five-model ensemble from the EU-Horizon2020 project PRIMAVERA covering a wide range of resolutions from 1° to 0.25°.

In section 2, we derive the water budget of tropical cyclones and describe the models of the PRIMAVERA ensemble. The results are presented in section 3 and discussed in section 4. We conclude and offer some perspectives in section 5.

2. Data and methods

a. *Computation of the water budget of tropical cyclones*

The conservation of moisture in the Eulerian frame of reference can be written in the pressure coordinate system as

$$\frac{\partial \rho q}{\partial t} + \nabla \cdot (\mathbf{u}\rho q) = e - c, \tag{1}$$

where $\mathbf{u} = (u_x, u_y, \omega)$ is the 3D velocity, where the scalar fields are a function of (x, y, p), e is the local evaporation, c is the local condensation, ρ is the density, and q is the specific humidity. By integrating Eq. (1) vertically, we obtain

$$\int_0^{p_s} \frac{\partial q}{\partial t}\frac{dp}{g} + \int_0^{p_s} \nabla_h \cdot (\mathbf{u}_h q)\frac{dp}{g} = E - P, \tag{2}$$

where p_s is the surface pressure, E is the surface evaporation, and P is the precipitation rate at the surface. We can decompose the horizontal velocity into

$$\mathbf{u}_h(x, y) = \mathbf{U} + \mathbf{u}'(x, y), \tag{3}$$

with $\mathbf{U}$ being the mean motion of the storm and $\mathbf{u}'$ the storm relative wind. As $\mathbf{U}$ is not a function of x and y, it follows that $\nabla_h \cdot \mathbf{U} = 0$. The total humidity of the air column is given by

$$Q = \int_0^{p_s} q\frac{dp}{g}. \tag{4}$$

The horizontal moisture flux convergence can be decomposed into a contribution due to the advection by the mean motion of the storm and a contribution due to the convergence by the anomalous circulation, as follows:

$$\int_0^{p_s} \nabla_h \cdot (\mathbf{u}_h \rho q)\frac{dp}{g} = \mathbf{U} \cdot \nabla_h Q + \int_0^{p_s} \nabla_h \cdot (\mathbf{u}'\rho q)\frac{dp}{g}. \tag{5}$$

By making use of Eqs. (2), (4), and (5) this gives

$$\frac{\partial Q}{\partial t} + \mathbf{U} \cdot \nabla_h Q + \int_0^{p_s} \nabla_h \cdot (\mathbf{u}'\rho q)\frac{dp}{g} = E - P. \tag{6}$$

We can write the derivative following the motion of the storm: $d/dt = (\partial/\partial t) + \mathbf{U} \cdot \nabla_h$, which should not be confused with the Lagrangian derivative, $d/dt = (\partial/\partial t) + \mathbf{u}_h \cdot \nabla_h$. In addition, we write $\mathbf{F} = \int_0^{p_s} \mathbf{u}'\rho q(dp/g)$, where $\mathbf{F}$ is the moisture flux in the frame of reference of the storm.

The tendency of moisture at a given time t is evaluated as the rate of change of the vertically integrated specific humidity between the observation immediately before and immediately after the time t. We project $\mathbf{F}$ onto the unit vectors of the cylindrical coordinates system in the frame of reference of the storm $\mathbf{F} = (F_r, F_\theta)$. All quantities are regridded in the cylindrical coordinates system and averaged azimuthally so that Q, F_r, E, and P are now only a function of r. We finally obtain

$$2\pi r \times \frac{dQ(r)}{dt} = 2\pi r \times \left[\int_0^{p_s} \frac{1}{r}\frac{\partial r F_r(r)}{\partial r}\frac{dp}{g} - E(r) + P(r)\right]. \tag{7}$$

Note that, by construction of the budget, all terms tend to 0 at the center of the storm (as the surface of a ring is infinitely small), and this should not be confused with dry conditions prevailing in the eye of the tropical cyclone. Getting a closed budget is particularly difficult when it is calculated from both instantaneous (wind, specific humidity) and accumulated (precipitation) values and when derivatives are estimated by finite

Downloaded from http://journals.ametsoc.org/jcli/article-pdf/33/19/8457/4995419/jcli190099.pdf by guest on 16 September 2020

TABLE 1. Description of the PRIMAVERA model ensemble.

Model	CMCC-CM2	CNRM-CM6-1	EC-Earth3P	ECMWF-IFS	HadGEM3-GC3.1
LR grid (resolution at equator)	1° × 1° (100 km)	Tl127 (156 km)	Tl255 (78 km)	Tco199 (50 km)	N96 (208 km)
HR grid (resolution at equator)	0.25° × 0.25° (28 km)	Tl359 (55 km)	Tl511 (39 km)	Tco399 (25 km)	N512 (39 km)
Dynamical core	Finite volume	Spectral	Spectral	Spectral	Finite difference
Convective parameterization	Neale et al. (2010)	Bougeault (1985)	Bechtold et al. (2001)	Bechtold et al. (2001)	Gregory and Rowntree (1990)

differences. In addition, errors in the evaluation of the term dQ/dt might arise if the distance traveled by the storm is larger than the grid cell size (i.e., if $U \times dt > dx$).

b. Tropical cyclone precipitation

Tropical cyclone precipitation is averaged in a radial cap of radius X measured along a great circle following the method used in Scoccimarro et al. (2014) and denoted TCP_X.

c. Objective tracking algorithm

Tropical cyclones have been tracked using the objective tracking algorithm TRACK (Hodges et al. 2017). The algorithm uses 6-hourly relative vorticity averaged over three levels (850, 700, and 600 hPa). Relative vorticity is filtered using a spectral truncation of T63. The algorithm locates centers of high relative vorticity ($>5 \times 10^{-6}\,\mathrm{s}^{-1}$), which we call tropical vortices. Only storms with a lifetime longer than two days are retained. The vertical structure of storms is scanned to select only those with a warm core structure. The same criteria were used in all basins. Final tracks are available four times a day, at 0000, 0600, 1200 and 1800 UTC. The same version of the TRACK algorithm was used in Roberts et al. (2020). In addition to all the criteria mentioned above, we select only cyclones in the band 40°N/S to discard cyclones that would retain a warm core while already exhibiting some baroclinic features. Typically, when TRACK is applied to a reanalysis, it identifies ~30 000 tropical vortices per year globally, ~8000 of which have a duration longer than two days, and ~120 of which have a warm core structure.

d. The PRIMAVERA model ensemble

The TC analysis is based on an ensemble of five GCMs that took part in the EU-Horizon2020 project PRIMAVERA (i.e., Process-based climate simulation: Advances in high-resolution modelling and European climate risk assessments; https://www.climateurope.eu/primavera/): CMCC-CM2 (Cherchi et al. 2019), CNRM-CM6-1 (Voldoire et al. 2019), EC-Earth3P (Haarsma et al. 2020), ECMWF-IFS (C. D. Roberts et al. 2018), and HadGEM3-GC3.1 (M. J. Roberts et al. 2018). Simulations follow the AMIP protocol and have been forced by HadISST2 daily sea surface temperature (SST) at a resolution of 0.25° reinterpolated to the model grid. We briefly summarize the characteristics relevant to each model in Table 1. Hereafter, the lower resolution of each GCM is abbreviated LR, and the higher resolution is abbreviated HR. Tropical cyclones in each simulation have been tracked using TRACK and the results of the tracking are discussed in Roberts et al. (2020). In the various models, precipitation is accumulated over 3 or 6 h, with different time windows for precipitation accumulation, and is not necessarily centered on the time at which the tracking is performed: for instance precipitation associated with the tracking time 0600 UTC is accumulated over the time range 0300–0600 UTC in HadGEM3-GC3.1 and CNRM-CM6-1, 0430–0730 UTC in EC-Earth3P, 0000–0600 UTC in ECMWF-IFS, and 0003–0900 UTC in CMCC-CM2. The moisture budgets analyzed in section 3c, which are near closure, suggest that the time period over which precipitation is accumulated does not introduce large errors in the budget term.

e. Observational products

For verification we use four reanalysis products: JRA-55 (Kobayashi et al. 2015) covering the time period 1958–2017, MERRA-2 (Gelaro et al. 2017) covering 1980–2018, ERA-Interim (Dee et al. 2011) covering 1980–2016, and ERA5 (Copernicus Climate Change Service 2017) covering 1950–2018. Precipitation in ERA-Interim and ERA5 is estimated from forecasts initialized from the analysis. In ERA-Interim precipitation is accumulated over 3 h after a 12-h lead time, whereas in ERA5 precipitation is accumulated over 1 h after a 6- or 12-h lead time depending on the time of the day (this is because ERA5 has only two forecast initial dates per day and ERA-Interim has four). Each reanalysis has been tracked independently with the TRACK algorithm.

For reference, TCP has also been computed in satellite products, TRMM3B42 (Huffman et al. 2007) covering 1998–2017 and CMORPH (Joyce et al. 2004) covering 2003–18 associated with TC tracks from IBTrACS

Downloaded from http://journals.ametsoc.org/jcli/article-pdf/33/19/8457/4995419/jcli190099.pdf by guest on 16 September 2020

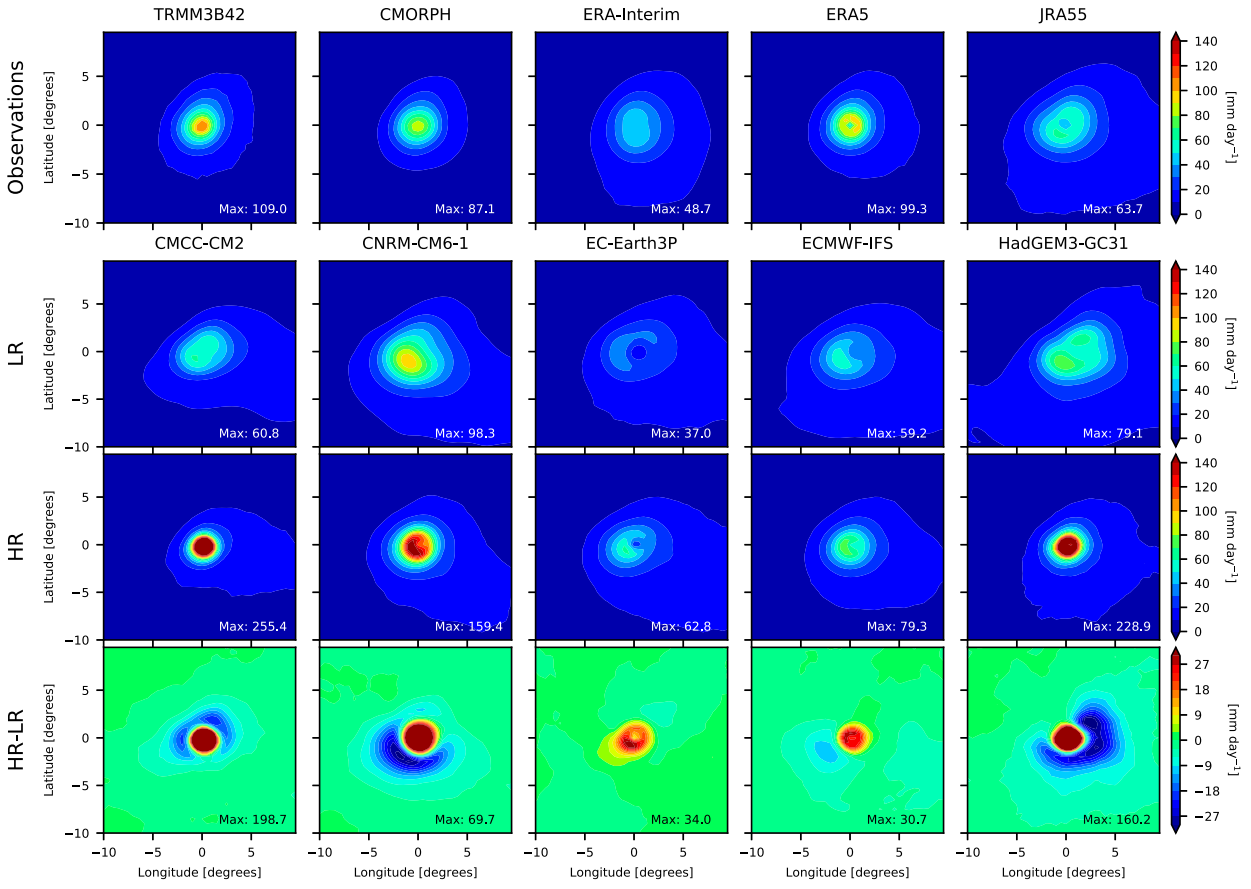

FIG. 1. Composite of precipitation (mm day^{-1}) for the 200 strongest TCs in the North Hemisphere over the period 1998–2014. The composites are centered on MSLP. (first row) Observations and reanalyses, (second row) LR, (third row) HR, and (fourth row) difference between HR and LR.

(Knapp et al. 2010). Precipitation has been averaged over three hours.

QScat-R is a dataset of tropical cyclone radial structure based on the near-surface ocean wind vectors from the QSCAT satellite (Chavas and Vigh 2014).

3. Results

a. Climatology of tropical cyclone precipitation

Figure 1 shows the composited precipitation for the 200 strongest tropical cyclones in each model over the period 1998–2014. We choose this time period because it is common to all models and most observational products. Precipitation has been averaged over the full lifetime of all the storms. This mean view is not representative of a single tropical cyclone, which is characterized by mesoscale structures, such as spiraling rainbands; rather, it reflects the likelihood of precipitation occurring at a given distance from the center of the storm. Three models show an increase of precipitation in the core region (HadGEM3-GC3.1, CNRM-CM6-1, and CMCC-CM2) and a decrease in the outer region (i.e., from a radial distance of 2° to 5°), which is consistent with TCs having a more compact structure at HR. In those three models, the extent of precipitation in the HR composite is in better agreement with TRMM3B42. ECMWF-IFS and EC-Earth3P, which share the same atmospheric component (IFS), show only an intensification of precipitation near the core. Note that the structure of TCs is more elongated in the LR of CMCC-CM2 and HadGEM3-GC3.1; this is possibly due to the coarser resolution in the zonal direction than in the meridional direction at low latitudes.

From Fig. 1, it appears that most precipitation associated with tropical cyclones occurs within 5° from the center of the storm for all models and resolutions considered. This motivates the use of a 5° radial cap to capture the total precipitation associated with tropical cyclones similar to that chosen by Trenberth et al. (2007) and Bacmeister et al. (2016), which we call $TCP_{5°}$.

In Fig. 2, the distribution of $TCP_{5°}$ is shown for observations (TRMM3B42 and CMORPH precipitation

Downloaded from http://journals.ametsoc.org/jcli/article-pdf/33/19/8457/4995419/jcli190099.pdf by guest on 16 September 2020

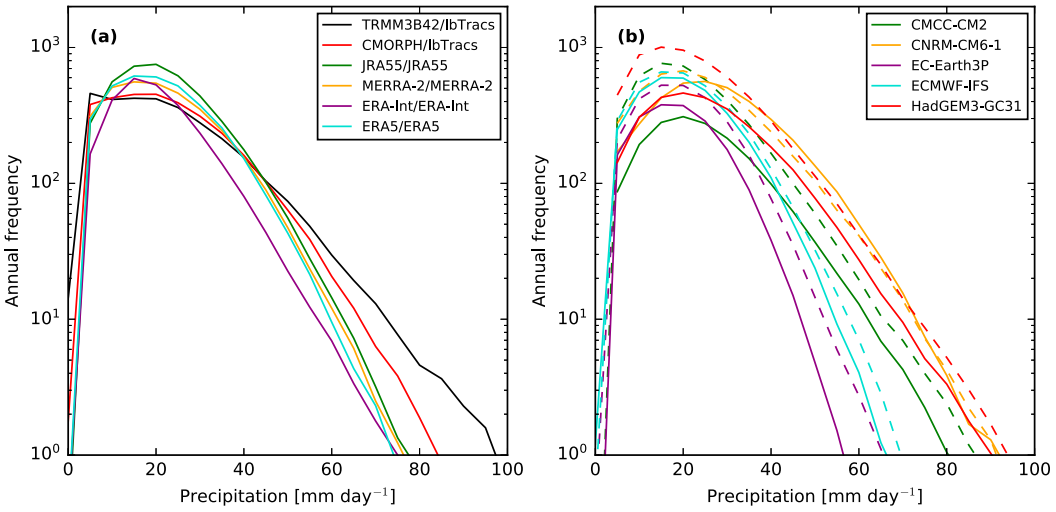

FIG. 2. Mean annual frequency of $TCP_{5°}$ in bins of 5 mm day^{-1} in (a) observations and (b) models. In (a) the legend indicates the pair of products used for precipitation and tropical cyclones tracks. Each 6-hourly observation counts for one occurrence. The entire time period available for each model and observation was used to compute the annual mean distribution. Solid lines stand for LR and dashed lines stand for HR.

associated with IBTrACS tracks) and reanalyses. There is a remarkable agreement of the distribution between JRA-55, MERRA-2, and ERA5, but ERA-Interim tends to underestimate the frequency for all bins (Fig. 2a). In CMORPH and TRMM3B42 associated with IBTrACS, the frequency of large $TCP_{5°}$ is higher than in reanalyses. On average TCP58 can reach 100 mm day^{-1} once a year in TRMM3B42 but it does not exceed 80 mm day^{-1} in reanalyses and CMORPH. The distribution of $TCP_{5°}$ in the models (Fig. 2b) overall covers the same range as in the observations and reanalyses. We find a larger impact of resolution for low-intensity $TCP_{5°}$ than for high-intensity $TCP_{5°}$ and we will explain why this is the case in the following paragraphs.

We hypothesize that the reduction of frequency of low-intensity $TCP_{5°}$ in LR (Fig. 2b) is explained by a lesser number of weak tropical storms reaching the threshold for warm core identification. This is confirmed by recomputing the distribution of precipitation for all tropical vortices (i.e., vortices identified before the warm core identification and the 2-day duration criterion). Note that tropical vortices capture between 45% and 60% of all tropical precipitation in the various models of PRIMAVERA (not shown). The distribution of precipitation averaged in a 5° cap shows much reduced differences of frequency between LR and HR at lower precipitation rates when tropical vortices are considered instead of TCs (Fig. 3). This result indicates that other convective systems, not identified as warm core TCs, do compensate for the lack of low intensity $TCP_{5°}$ in LR models.

Interestingly, the high-intensity $TCP_{5°}$ has a larger intermodel spread than a change with resolution for each model taken individually (Fig. 2b). This is in contrast with the large impact of resolution on the frequency of the minimum sea level pressure (MSLP) in CMCC-CM2, CNRM-CM6-1, and HadGEM3-GC3.1 (Fig. 4b). The difference in sensitivity to resolution of intense $TCP_{5°}$ and deepest MSLP is counterintuitive as one would imagine that intense tropical cyclones generate larger precipitation rates. It will be an important focus of this paper to reconcile the two seemingly contradicting results.

Also investigated is whether the impact of resolution on TCP varies from one ocean basin to another. Figure 5 shows maps of annual precipitation associated with tropical cyclones in a 5° cap. An increase of $TCP_{5°}$ occurs in all models and all basins when resolution increases (Fig. 6, left column). This increase is larger in CMCC-CM2 and HadGEM3-GC3.1 than in EC-Earth3P and ECMWF-IFS and follows a more complex pattern in CNRM-CM6-1, with a decrease in the tropical band and an increase poleward.

To further understand the role of TCP and TC frequency in setting the change of P with resolution, we decompose

$$P(x,y) = \mathrm{TCP}(x,y) \times f_{\mathrm{TC}}(x,y), \tag{8}$$

where P represents the total precipitation associated with tropical cyclones per year at longitude and latitude (x, y), TCP the mean precipitation per tropical cyclone,

Downloaded from http://journals.ametsoc.org/jcli/article-pdf/33/19/8457/4995419/jcli190099.pdf by guest on 16 September 2020

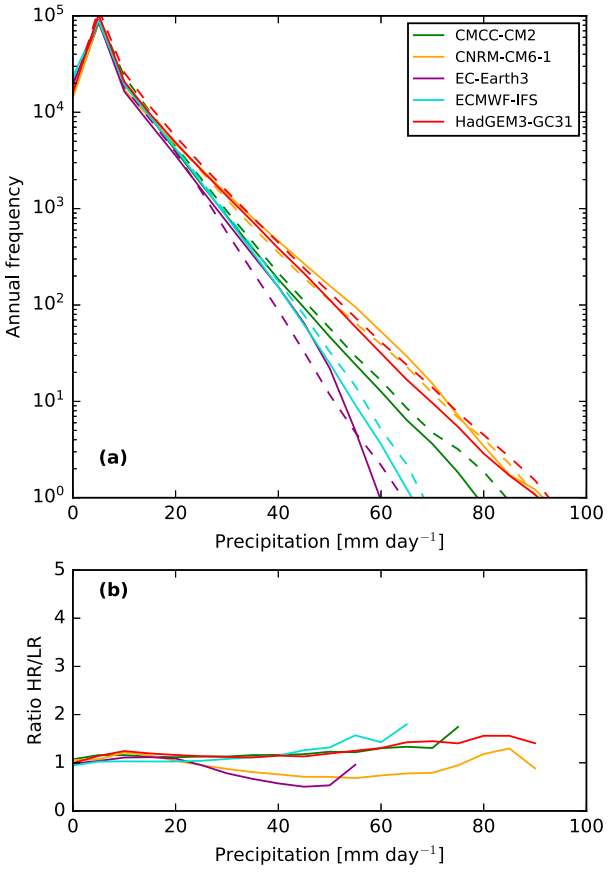

FIG. 3. (a) As in Fig. 2b, but for precipitation associated with all tropical vortices within a radius of 5° from MSLP and (b) the ratio of the distribution between HR and LR.

and f_{TC} the frequency of a grid point being overlapped by a TC 5° cap. By differentiating Eq. (8), we obtain

$$\Delta P = P \times \left(\frac{\Delta \mathrm{TCP}}{\mathrm{TCP}} + \frac{\Delta f_{TC}}{f_{TC}} \right), \tag{9}$$

where Δ represents the difference between HR and LR. The two terms on the right-hand side correspond respectively to the contribution of the fractional change of precipitation per tropical cyclone and the fractional change of TC frequency to the change in total precipitation associated with TCs. The result of this decomposition is shown in Fig. 6 (middle and right columns). We find that ΔP is mostly explained by the change in frequency of tropical cyclones when resolution is increased. In HadGEM3-GC3.1, CNRM-CM6-1, and CMCC-CM2, it is slightly offset by a decrease in the amount of precipitation per TC. This is easily understood by the reduction of frequency of low-intensity $TCP_{5°}$ in LR, discussed previously, which leads to higher $TCP_{5°}$ when averaged over all bins.

b. Tropical cyclone core precipitation

In Fig. 7, we analyze the distribution of precipitation occurring at the core of tropical cyclones by averaging precipitation in a 1° cap ($TCP_{1°}$) in reanalyses and models. $TCP_{1°}$ with a frequency of one observation a year has an intensity ranging from 300 to 400 mm day^{-1} in the various observational products. However the same quantity has a much larger spread in models, ranging from 130 to 500 mm day^{-1}. Thus, contrary to $TCP_{5°}$, $TCP_{1°}$ is strongly affected by resolution. This is even more true in models that are able to reach very large intensities such as CMCC-CM2, CNRM-CM6-1, and HadGEM3-GC3.1 (Fig. 2), suggesting a possible link between the ability of models to develop large rain rates in the core region and to simulate deep MSLP.

We now tentatively make a parallel between the ability of models to reach intense $TCP_{1°}$ and gridpoint extreme precipitation. Because core precipitation occurs over a small area, it relates more directly to extreme precipitation metrics defined at the gridpoint scale than precipitation averaged in the whole tropical cyclone does. Interestingly, Bador et al. (2020) found that HadGEM3-GC3.1 and CMCC-CM2 produce the largest change with resolution of the following extreme precipitation metrics: maximum 1-day precipitation (rx1day), maximum 5-day precipitation (rx5day), and total precipitation from extremely wet days (r99p), over both land and ocean, suggesting that tropical cyclone core precipitation in these models share essential physics with processes that contribute to set the extreme precipitation captured by those three metrics.

c. Moisture budget of tropical cyclones

Focusing on the most intense tropical cyclones rather than cyclones of a given intensity to evaluate the role of resolution on the moisture budget of TCs appears to be the best approach, since we showed in section 3a that there was no obvious relationship between $TCP_{5°}$ and the MSLP. The water budget of tropical cyclones has been computed [following Eq. (7)] for the same selection of 200 strongest cyclones used for Fig. 1 but at the time of minimum MSLP only. The contribution of each term of the budget between two radii can be interpreted as the area below the curve and between those two radii (Fig. 8). For all models and all resolutions and at radial distances less than 5°, the main balance is between moisture convergence and precipitation. Surface evaporation within 500 km contributes only 10%–15% of the moisture ultimately condensed in TCs. Following Trenberth et al. (2007), we estimate the radius of the moisture source for each composite, defined as the distance at which evaporation needs to be integrated from

Downloaded from http://journals.ametsoc.org/jcli/article-pdf/33/19/8457/4995419/jcli190099.pdf by guest on 16 September 2020

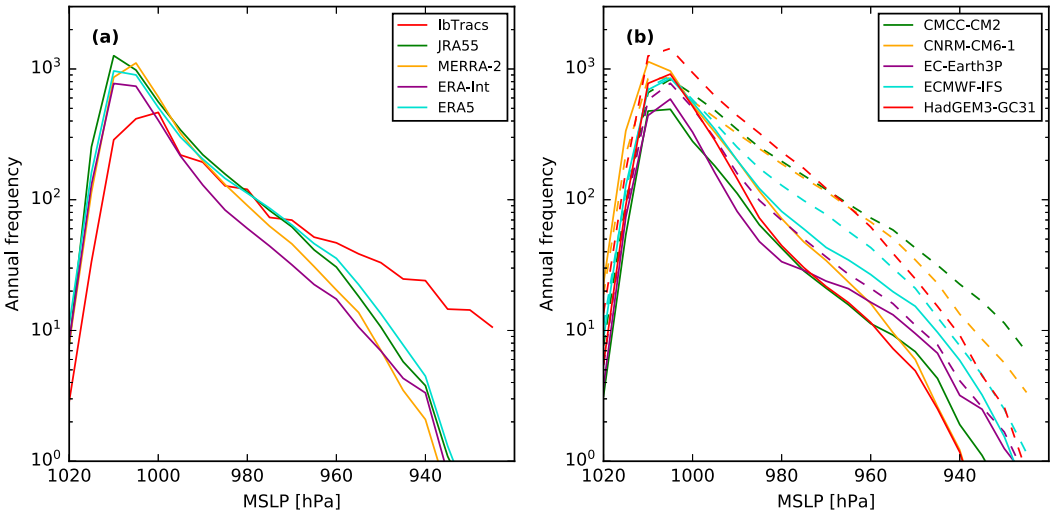

FIG. 4. As in Fig. 2, but for the mean annual frequency of MSLP in bins of 10 hPa in (a) observations and (b) models.

the center of the storm to find the same amount of water as $TCP_{5°}$. The estimated radii in the PRIMAVERA ensemble are in the range 1297–1528 km (see Fig. S1 in the online supplemental material). The radii of the moisture source are smaller in ECMWF-IFS and EC-Earth3P than in the other three models. The estimated radii are also slightly smaller than the 1600 km found by Trenberth et al. (2007) in the case study of Ivan and

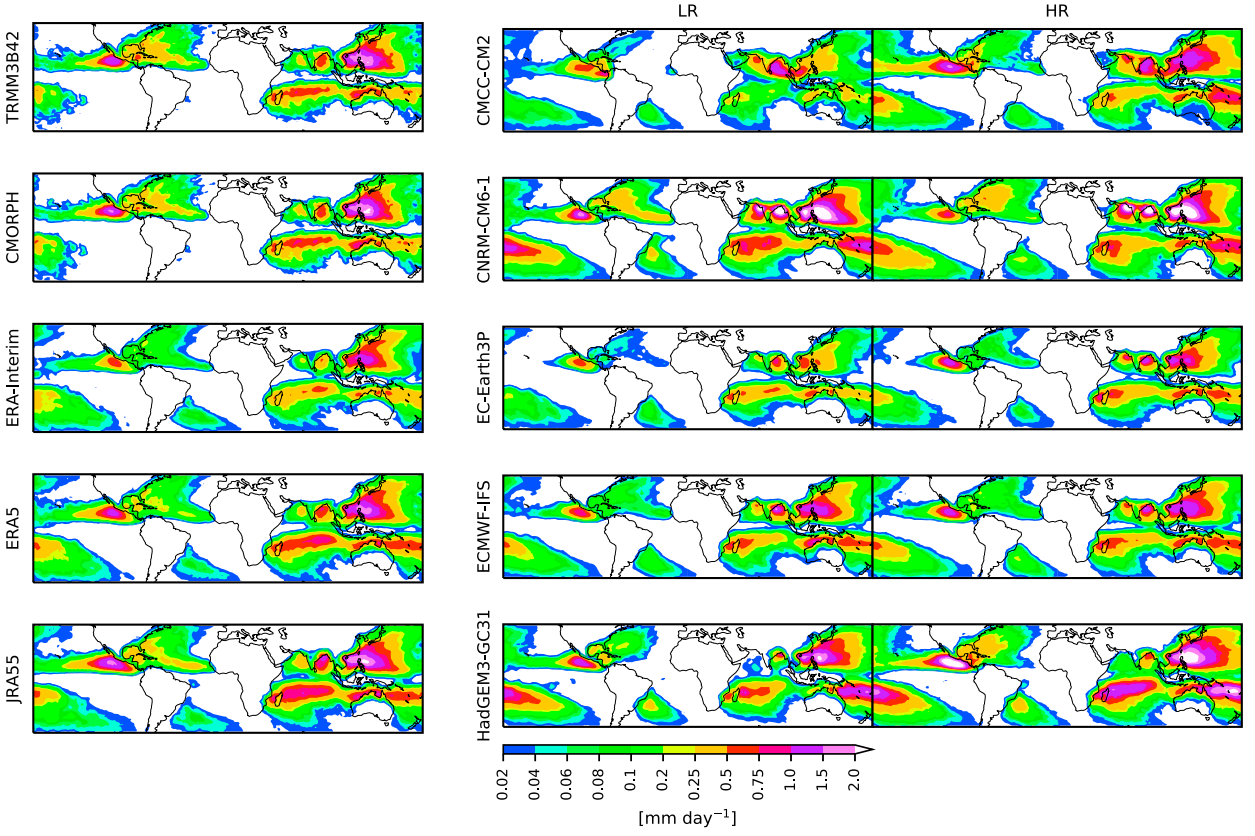

FIG. 5. Precipitation associated with tropical cyclones (mm day^{-1}; occurring in a 5° cap) in (left) TRMM3B42/IBTrACS, CMORPH/IBTrACS, ERA-Interim, ERA5, and JRA-55, (center) LR models, and (right) HR models.

Downloaded from http://journals.ametsoc.org/jcli/article-pdf/33/19/8457/4995419/jcli190099.pdf by guest on 16 September 2020

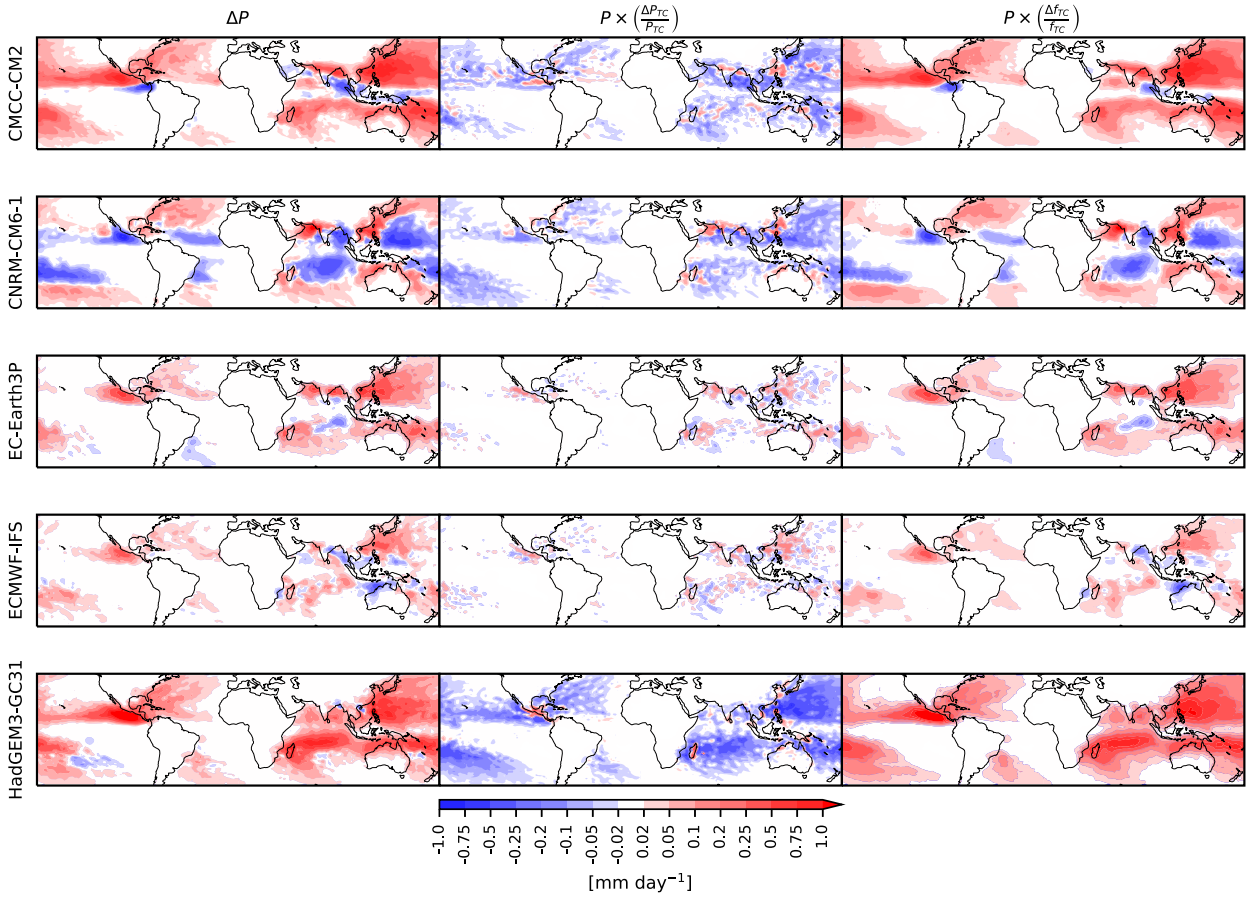

FIG. 6. (left) Difference of precipitation associated with tropical cyclones (mm day^{-1}; occurring in a 5° cap) between HR and LR. Precipitation associated with tropical cyclones (occurring in a 5° cap). The difference of precipitation between HR and LR has been decomposed into two contributions resulting from (center) the change in the amount of precipitation per tropical cyclone and (right) the change of the number of tropical cyclones.

Katrina with WRF at a resolution of 4 km. The exceptional intensity of those two TCs compared to the 200 selected in the model composites could explain this difference.

When resolution increases, there is a clear redistribution of moisture flux convergence toward the core of the TC and as a result a redistribution of precipitation in CMCC-CM2, CNRM-CM6-1, and HadGEM3-GC3; there is however no marked change of the total precipitation between 0° and 5° in HadGEM3-GC3 and CNRM-CM6-1. In ECMWF-IFS and EC-Earth3P, there is little sensitivity of precipitation and moisture flux convergence to resolution. Despite having the highest resolution of the ensemble, ECMWF-IFS HR precipitation is closer to that of its LR configuration. This cannot be solely explained by the fact that IFS is a spectral model as CNRM-CM6-1 is also a spectral model, based on a former version of the IFS dynamical core. The lack of resolution sensitivity is also found in ERA-Interim and ERA5 (which have the same resolution difference as between EC-Earth3P LR and HR) despite more data being assimilated in ERA5.

We further decomposed the terms of the moisture budget and found that the moisture flux due to the displacement of the storm has a very small amplitude compared with the moisture fluxes due to the anomalous circulation (not shown). This is unlike the displacement of moisture by extratropical cyclones, which becomes important poleward of 40°N/S with respect to the other terms of the moisture budget (Dacre et al. 2015) and can be explained by the large increase of cyclones translation speed at higher latitudes. In addition, we split the divergence of the moisture flux due to the anomalous circulation [i.e., the third term on the lhs of Eq. (6)] into the advection of moisture by the anomalous circulation and the product of humidity and mass divergence. We find that the advection offsets slightly the term associated to mass divergence but we do not show this decomposition as it does not bring additional insight.

Downloaded from http://journals.ametsoc.org/jcli/article-pdf/33/19/8457/4995419/jcli190099.pdf by guest on 16 September 2020

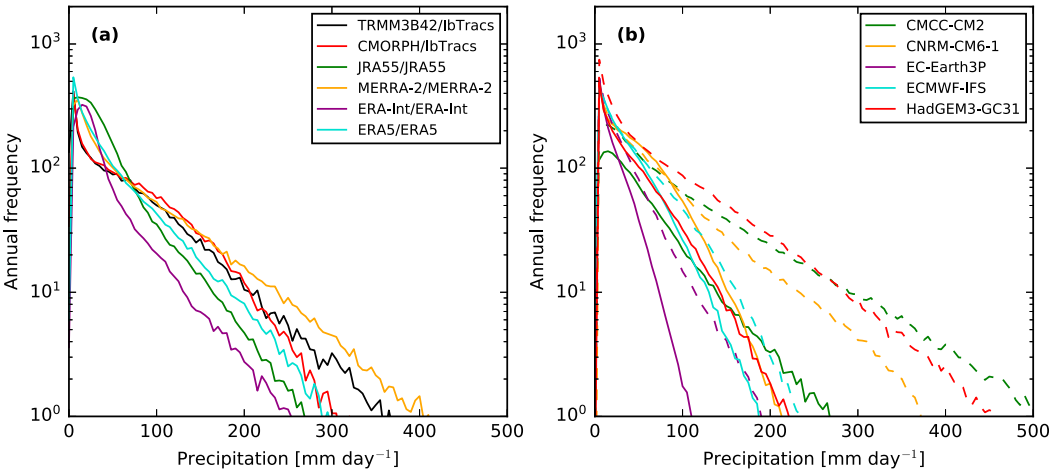

FIG. 7. As in Figs. 2a and 2b, but for $TCP_{1°}$.

Next, the role that low-level wind might play in the redistribution of moisture is explored. In Fig. 9, we have decomposed the wind profile into its azimuthal and radial components. The composited wind profiles of GCMs have been compared with a QScat-R composite built in an analogous way. We identified the 200 strongest events in the Northern Hemisphere in IBTrACS over the period 1998–2014. We have selected the TCs in

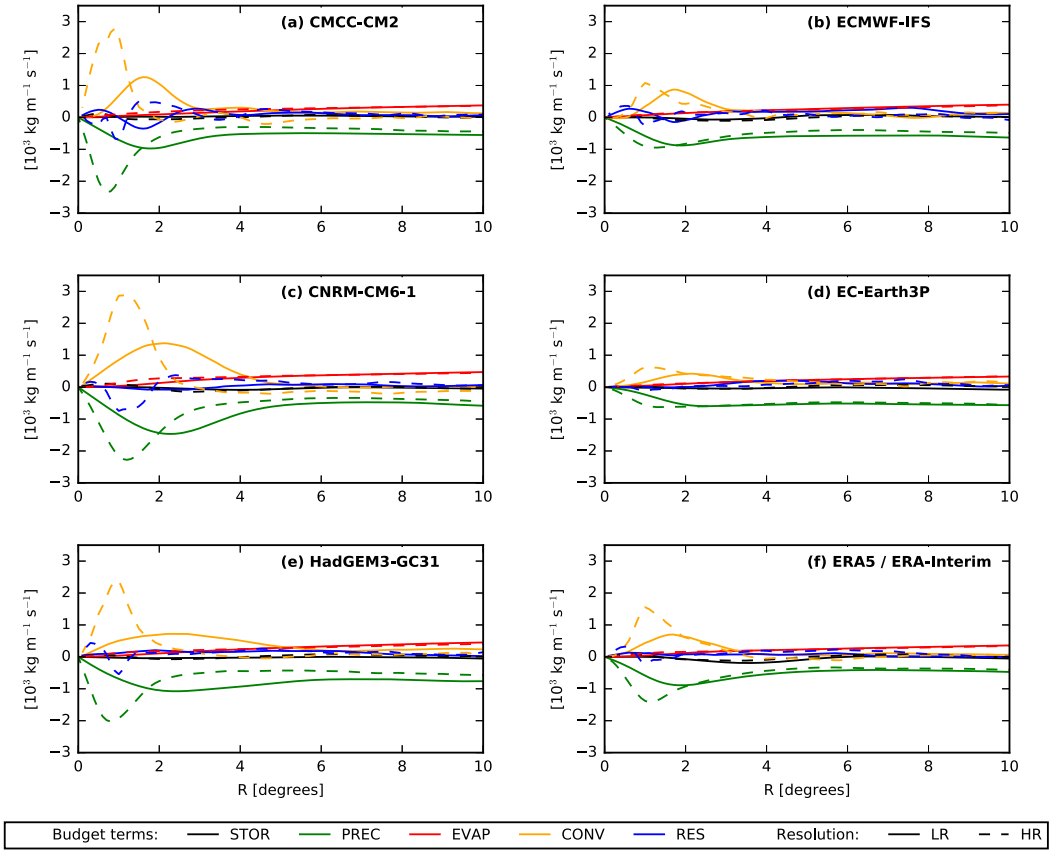

FIG. 8. Composite of the 200 strongest TCs in the North Hemisphere over the period 1998–2014 and at time of minimum MSLP. The components of tropical cyclones water budget are azimuthally and vertically averaged for a small ring of width *dr* at distance *r* from the center of the storm. The components are of the budget (kg m^{-1} day^{-1}) are the storage (STOR), the moisture flux convergence (CONV), precipitation (PREC), evaporation (EVAP), and the residual (RES). LR models are represented by solid curves and HR by dashed curves.

Downloaded from http://journals.ametsoc.org/jcli/article-pdf/33/19/8457/4995419/jcli190099.pdf by guest on 16 September 2020

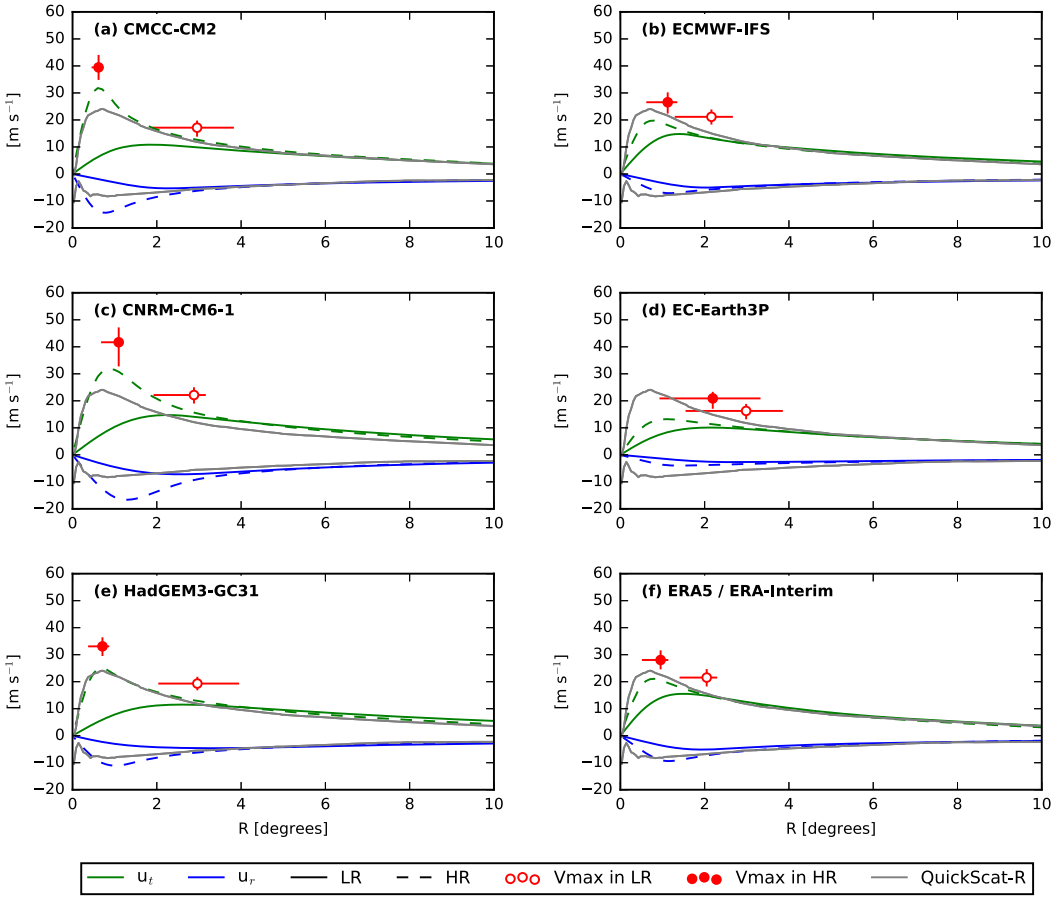

FIG. 9. Composite of the 200 strongest TCs in the North Hemisphere over the period 1998–2014 and at time of minimum MSLP. Mean (green) azimuthal and (blue) radial wind components at 10 m for LR (solid) and HR (dashed). Open (solid) red markers indicate the maximum 10-m wind in LR (HR) averaged in the composite and the bars indicate the 25% and 75% percentiles of the distance from the center and intensity of maximum wind in the composite.

this composite that appear in QScat-R. As QScat-R only covers the period 2000–09, this results in less TC being retained in the composite (107). The sensitivity of the TCs low-level wind to resolution varies among models. At the surface, there is a marked increase of the mean azimuthal wind in CMCC-CM2, CNRM-CM6-1, and HadGEM3-GC3.1, together with a displacement of the strongest azimuthal wind toward the center of the storm. Moreover, there is a relatively good agreement between the wind profile at HR in CMCC-CM2, CNRM-CM6-1, HadGEM3-GC3.1, and ERA5 with QScat-R. However, in ECMWF-IFS and EC-Earth3P, there is only a moderate change of the surface wind with resolution. We also indicate in Fig. 9 the position and intensity of the maximum wind before the azimuthal averaging (red markers). In CMCC-CM2, CNRM-CM6-1, and HadGEM3-GC3.1, there is a larger increase of the maximum wind speed and a larger displacement of the position of this maximum toward the center of the storm than in the two models using IFS. The position is also better constrained with a reduction of the variance of the composite.

The surface radial wind profiles converge in LR and HR at around 5° in all models. At low levels, the radial wind at 5° plays a key role together with specific humidity in setting the moisture inflow into the tropical cyclone. This is consistent with the fact that the mean precipitation per TC differs little between LR and HR. However, the change in the radial wind within the cap means that moisture will be redistributed differently, with the stronger radial wind in HR leading to more moisture being advected closer to the core.

To ascertain the control of the radial wind at the edge of the cap on precipitation, we investigate the correlation between the two quantities in the composite of TCs. Not only do we find a strong correlation between the low level radial wind at the edge of a 5° radial cap (i.e., wind taken at 925 hPa and 5° from the center of the storm) and $TCP_{5°}$ in each model and resolution (Fig. 10a), but all

Downloaded from http://journals.ametsoc.org/jcli/article-pdf/33/19/8457/4995419/jclid190999.pdf by guest on 16 September 2020

models and resolutions fall on a similar regression line. Moreover, we find that the low-level radial wind at the edge of the cap has a larger intermodel variability than sensitivity to resolution (Fig. 10a). To contrast the role of the large-scale moisture balance with the intensification of the storm itself in setting $TCP_{5°}$, we also represent $TCP_{5°}$ against MSLP in Fig. 10b. As anticipated from the previous sections, the relation between $TCP_{5°}$ and MSLP shows a larger change with resolution than with model formulation. Note also that for a given TC intensity, LR produces more precipitation than HR. These results confirm the large-scale control of the water budget of tropical cyclones and shows it is only weakly related to tropical cyclone intensity.

d. Moist processes and tropical cyclone energetics

Several studies have emphasized that, despite representing a small contribution to the tropical cyclone moisture budget, the latent heat flux nonetheless plays a crucial role, as it modifies the specific humidity and equivalent potential temperature and destabilizes the atmospheric column (Malkus and Riehl 1960; Arakawa 2004). It is possible that, although it makes a negligible change in the moisture budget, the increase of surface latent heat flux in HR can strengthen cyclogenesis. In Fig. 11, an attempt is made to give an overview of the role of moist processes in setting the storm intensity.

Even LR models can capture the equivalent potential temperature θ_e structure characterizing tropical cyclones: an inward increase of absolute momentum at low levels and an outward slope of moist adiabat above the boundary layer (Emanuel 2018). In the core region, isocontours of absolute momentum are aligned with moist adiabats, suggesting slantwise convective adjustment has occurred, despite the parameterization of convection removing upright convective instability. The lines of absolute momentum form a sharper gradient in the core region in HR models as expected from more intense TCs. The difference of θ_e between LR and HR shows a column of anomalously warm air in the core region in all models, whereas the sign of the anomaly away from the core varies among models. Models with the warmest core anomaly are those developing the deepest MSLP: CNRM-CM6-1 and HadGEM-GC3.1.

The surface latent heat flux shows that the largest differences occur between LR and HR in the core region, a region which coincides with the largest wind anomalies (cf. Fig. 9). At first, those results might seem paradoxical with the moisture budget view presented in Fig. 8, where it was concluded that there was little sensitivity of surface latent heat flux with resolution. This is because the region of large anomalous latent heat, close to the center of the storm, makes a negligible contribution to

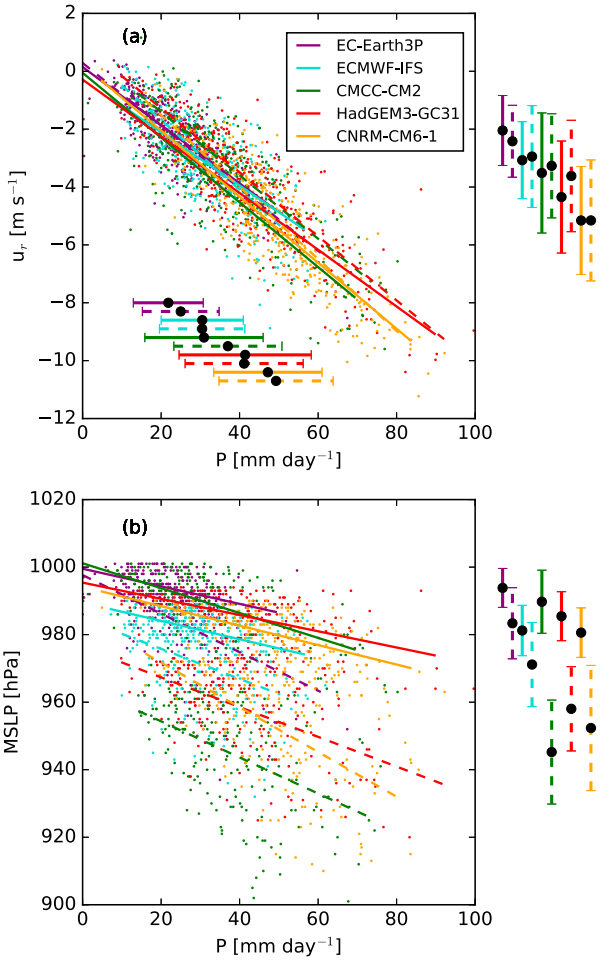

FIG. 10. Scatterplots of (a) radial wind at 925 hPa and 5° from the center of the storm and (b) MSLP vs precipitation averaged in a 5° radial cap for the composite of the 200 strongest TCs in the North Hemisphere over the period 1998–2014 and at time of minimum MSLP. Solid and dashed lines represent the fitted linear regression curves of LR and HR, respectively. The mean and the range of two standard deviations for the radial wind in (a) and MSLP in (b) are indicated on the right-hand side of each subplot for each model and each resolution (using the same line style coding as for the regression curves).

the moisture budget of the tropical cyclone. Finally, we note that the IFS-based models (i.e., ECMWF-IFS, EC-Earth3P, and the two reanalyses ERA-Interim and ERA5) have less sensitivity of surface latent heat flux to resolution.

The diagnostics presented in this section provide a good illustration of an enhanced intensification feedback at higher resolution (or WISHE feedback; Emanuel 1986). Indeed, stronger winds extract more latent heat from the ocean, and parcels taking up more moisture give rise to a larger inward increase of θ_e in the boundary layer and thus a warmer core, which ultimately maintains stronger winds. In IFS models, the intensification feedback has a lesser sensitivity to resolution. It has been suggested that the lateral diffusion of heat and

Downloaded from http://journals.ametsoc.org/jcli/article-pdf/33/19/8457/4995419/jcli190099.pdf by guest on 16 September 2020

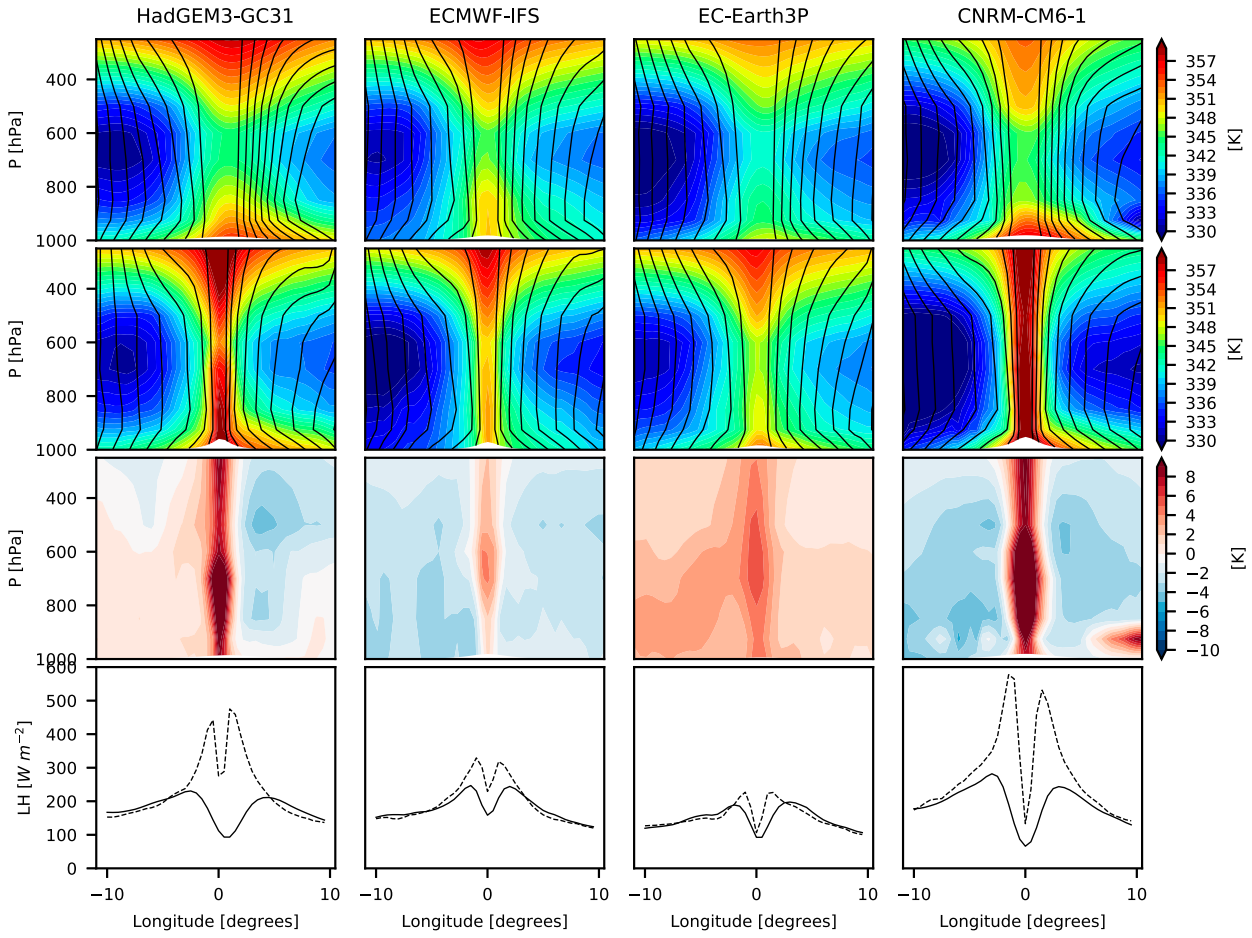

FIG. 11. Equivalent potential temperature θ_e (K; color) and iso-contours of absolute momentum M (black lines) for (first row) LR, (second row) HR, (third row) the difference between HR and LR, and (fourth row) surface latent heat flux (W m^{-2}).

momentum by parameterized three-dimensional turbulence and numerical truncation errors could alter θ_e gradients in the core region (Emanuel 2018). However, we note that IFS is a spectral model and has the ability to compute gradients with high accuracy. Moreover, Klaver et al. (2020) found that, at midlatitudes, IFS was the model of the PRIMAVERA ensemble with the highest effective resolution.

As emphasized by Emanuel (2018), in a similar way as for midlatitude frontogenesis, it is the secondary circulation of tropical cyclones that enhances the core temperature gradients. To evaluate if, for a given intensity of tropical cyclones, the secondary circulation has the right intensity, we calculated the cross-flow angle defined as $\tan^{-1}u_r/u_\theta$, with u_r and u_θ, the radial and azimuthal components of wind, respectively. The results are shown in Table 2. We find that the cross-flow angle in the outer region of the storm has little dependence on the resolution of climate models, which suggests it is intrinsically related to model formulation. For radii less than 2°, the dependence on resolution is larger, which is consistent with the core region with relatively weak wind occupying a larger area in LR models. The cross-flow angle is systematically lower in IFS-based models, both in the inner and the outer regions, suggesting that some essential model physics pertaining to TC intensification is misrepresented. The too weak secondary circulation in the IFS models will have consequences for both the intensification of TCs and their water budget. First, a too weak secondary circulation close to the core will not allow moist air to reach the innermost region of the TC, therefore hampering the intensification feedback described in the previous paragraph. Second, a too weak secondary circulation in the outer region will reduce the inward component of moisture fluxes at the edge of TCs, potentially explaining the smaller rain rate in the models using the IFS dynamical core (Fig. 2).

4. Discussion

We have analyzed the moisture budget of tropical cyclones in the multimodel PRIMAVERA ensemble.

Downloaded from http://journals.ametsoc.org/jcli/article-pdf/33/19/8457/4995419/jcli190099.pdf by guest on 16 September 2020

TABLE 2. Cross-flow angle (°) of wind at 925 hPa averaged for radii between 0° and 2° and radii between 2° and 5° from the center of the storm.

Radius	Resolution	CMCC-CM2	CNRM-CM6-1	EC-Earth3P	ECMWF-IFS	HadGEM3-GC3.1	ERA-Interim/ERA5
$0° < r < 2°$	LR	8.65°	10.97°	2.83°	4.27°	12.56°	5.18°
	HR	17.09°	14.33°	5.69°	7.72°	15.85°	8.13°
$2° < r < 5°$	LR	15.87°	16.65°	8.40°	11.45°	15.40°	11.48°
	HR	15.99°	19.18°	10.21°	12.36°	15.81°	13.10°

One puzzling result is that, while the intensity of tropical cyclones is strongly affected by a change in model resolution, by contrast there is very little impact of resolution on precipitation per TC. By contrasting a moist energetic view and a moisture budget view, our analysis provides explanations as to why there is little interdependence between the two.

Tropical cyclone intensity is better understood by analyzing the specific humidity as an intensive parameter, while the moisture budget does not give much insight for the storm energetics. The WISHE feedback loop is curbed in LR models, as they underestimate the chain of processes linking high-intensity wind with the extraction of large amounts of latent heat from the ocean, leading to the warming of the core. Either model resolution is simply not fine enough to represent processes occurring on the scale of a few tens of kilometers, or LR models could overly diffuse temperature gradients. Those results are consistent with those presented in Wing et al. (2019) showing that GCMs with a more intense surface flux feedback develop more intense tropical cyclones and that a large fraction of the intermodel spread in the representation of TCs is due to the interaction between spatially varying surface fluxes and developing TCs.

Tropical cyclone precipitation is well explained by the moisture budget view. Large-scale moisture advection is in balance with precipitation to first order, with local evaporation playing a secondary role. We found that there is little impact of resolution on the far wind field, which controls the amount of moisture converging into the cap. It is surprising that, contrary to what was surmised in the introduction, their supposedly better resolved mesoscale features do not modify the efficiency of convection within tropical cyclone systems. However, from the point of view of radiative convective equilibrium, the warming due to convective ascent, which balances radiative cooling, might be only weakly sensitive to resolution if we make the hypothesis of weak temperature gradients. Instead, our results suggest that the amount of precipitation occurring in tropical cyclones is the result of a large-scale balance, in good agreement with previous results (Trenberth et al. 2007).

We believe that two aspects of the methodology we used allowed us to reach the conclusion that TCP has little sensitivity to resolution: the compositing technique and the choice of the tracking algorithm.

First, we preferred to composite the 200 strongest TCs over a 17-yr period, rather than to stratify TCs by intensity as frequently done (Kim et al. 2018; Moon et al. 2020; Wing et al. 2019). Stratifying by intensity could have led us to a seemingly contradicting conclusion, as we showed in Fig. 10b that, for a given intensity, LR models produce more precipitation than HR. This is explained by the lack of a unique relation between MSLP and TCP, which all resolutions and models would satisfy. We believe that our approach is complementary to the aforementioned studies in assessing the impact of resolution on TCP.

Second, we believe the results could have been affected by the choice of a different tracking algorithm. Indeed, we found that the weakest TCP rates are less frequent in LR models than in HR. When all tropical vortices are considered, rather than only those identified as TCs with a warm core, such a difference disappears. This implies that tropical vortices, which are not identified as TCs, do compensate for the lack of rain due to missing TCs. In the light of this result, choosing TRACK seems particularly relevant, as it discards overly small features. The count of tropical cyclones appears even more sensitive to resolution when another tracking algorithm, TempestExtreme, using pointwise detection, was used for the tracking [see results by Roberts et al. (2020) and the description of the algorithm therein]. To illustrate this, the distribution of $TCP_{5°}$ was recomputed with the TC tracks computed by TempestExtreme in Fig. 12. The ratio of the distribution obtained with TempestExtreme and TRACK shows that the two tracking algorithms converge for the strongest $TCP_{5°}$, but weaker $TCP_{5°}$ is strongly underestimated by TempestExtreme. In addition, the TCP distribution obtained with the two tracking algorithms tends to be in better agreement at HR than at LR, which is consistent with findings by Roberts et al. (2020) showing the convergence at HR of the count of TCs identified by the two trackers.

The role of coupling has not been investigated in this study, yet it is known to exert a feedback on tropical cyclone intensity (Vincent et al. 2012a,b), which is likely

Downloaded from http://journals.ametsoc.org/jcli/article-pdf/33/19/8457/4995419/jcli190099.pdf by guest on 16 September 2020

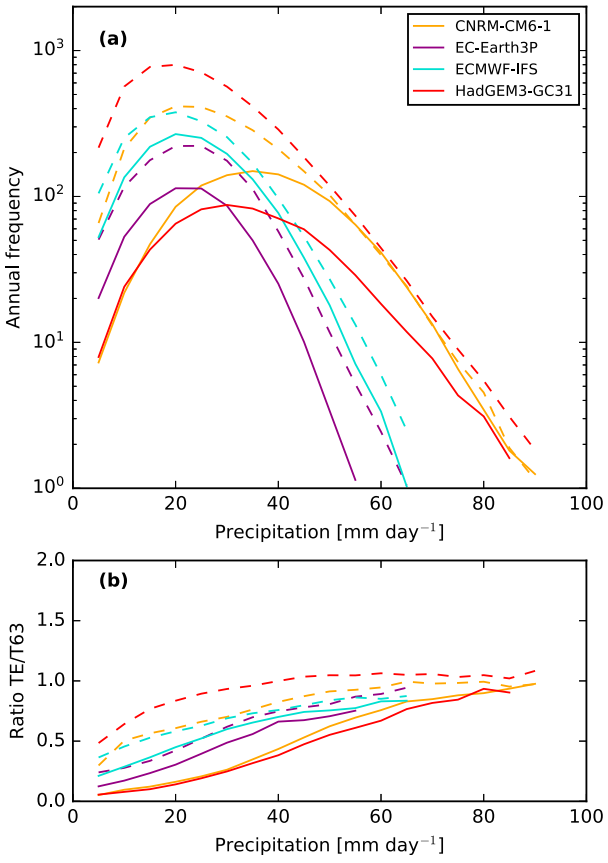

FIG. 12. (a) As in Fig. 2b, but for TCs tracked by the tracking algorithm TempestExtreme and (b) the ratio of the distribution of $TCP_{5°}$ for TCs tracked with TempestExtreme (TE) and TRACK (T63). Note that tropical cyclones in CMCC-CM2 have not been tracked with TempestExtreme.

to depend on horizontal resolution. One difficulty inherent to coupled experiments is to distinguish the role of coupling itself from the role of SST biases in altering the moisture budget and intensity of tropical cyclones. Atmospheric models coupled to slab ocean models might offer a solution to assess the role of the ocean response without the uncertainty arising from SST biases.

We found that sensitivity of TCs to resolution is low in IFS models, including in ECMWF-IFS and despite recent developments of IFS (cycle 43r1) to make the Charnock parameter used in the calculation of the exchange coefficient of momentum (Cd) dependent on the sea state, and although this modification resulted in a decrease of Cd at high 10-m wind speeds (Magnusson et al. 2019). However, a recent retuning of the Charnock parameter at high wind speeds, introduced in a later cycle 47r1, and not yet operational at the time of writing this paper, has shown the potential for further improvements, leading in particular to an increase of maximum surface wind speed and tropical cyclone intensity, but also to an increase in the amount of heat and moisture extracted from the ocean (Janssen and Bidlot 2018).

This work leaves several open questions for future research. First, several recent studies have discussed the spatial scale at which the atmospheric moisture budget is closed (Dagan et al. 2019) and the radiative–convective equilibrium (RCE) is reached (Jakob et al. 2019). Dagan et al. (2019) define this spatial scale as the distance at which the moisture flux divergence makes a negligible contribution to the moisture budget with respect to surface evaporation and precipitation. On annual time scales, the two studies find a similar spatial scale of 4000 km, which, we note, is roughly twice the radius at which the water budget of tropical cyclones is closed [Trenberth et al. (2007), and results presented in this study]. It would be interesting to understand in more detail if a climatology of tropical cyclones, as presented in this study, form a subset of events that could satisfy a similar spatial scale of closure to the atmospheric water budget, as calculated in Dagan et al. (2019).

Another open question is what determines the wind profile of tropical cyclones in GCMs. Indeed, one surprising result of this study is that, despite larger maximum wind near the core, the wind profile converges with resolution at large radii. The results presented in this paper can help gain insight into relevant physical mechanisms. One possible hypothesis to explain this behavior is that convection entrains air parcels from the large-scale environment with similar physical properties at high and low resolutions. Sufficiently far away from the center, the wind profile is set by the conservation of angular momentum of those parcels and is not altered by model resolution. Closer to the core, however, the wind profiles diverge in high and low resolution, either because the convective adjustment occurs before the parcels can reach the center at low resolution and/or because the radial temperature gradient is too diffuse.

5. Conclusions and perspectives

The general findings of the study are as follows:

1) Per-TC precipitation simulated in GCMs, unlike TC intensity, is relatively insensitive to the grid horizontal resolution. TC precipitation has however some dependence on model formulation.
2) Per-TC precipitation is in balance with the large-scale environment: the intensity of low-level radial wind at the edge of the tropical cyclone is well correlated with the amount of precipitation in tropical cyclones. This large-scale balance appears to be independent from the inner core dynamics and low- and high-resolution models capture it equally well.

Downloaded from http://journals.ametsoc.org/jcli/article-pdf/33/19/8457/4995419/jcli190099.pdf by guest on 16 September 2020

3) Despite having a negligible contribution to the moisture budget, the increase of surface latent heat flux near the core of TCs is part of a chain of processes leading to a larger TC intensification at high resolution.
4) The change in the radial wind profile with resolution leads to a redistribution of precipitation within the TC. This is true in particular in CNRM-CM6-1, CMCC-CM2, and HadGEM3-GC3.1, which achieve mean precipitation rates in the core of tropical cyclones as large as 500 mm day^{-1}, whereas in IFS-based models this is large, albeit to a lesser extent.
5) The impact of horizontal resolution on the contribution of TCs to global precipitation is largely due to a change in the number of tropical cyclones. This number is rendered uncertain by the choice of the tracking algorithm, the definition of TC identification criteria and the sensitivity of the algorithm itself to resolution.

Our results question the relevance of studying the water budget of tropical cyclones in small limited domains because the forcing prescribed at the boundaries could constrain this budget. Alternatively, the rotating radiative–convective equilibrium framework (Zhou et al. 2014, 2017) could be valuable to explore the impact of model resolution on the water budget of tropical cyclones: coupling the column physics of a GCM to a rotating hydrostatic dynamical core in a doubly periodic domain at varying resolutions would have the advantage of avoiding prescribing lateral boundary conditions and would seem relevant to understand the role of the large-scale environment on the water budget.

Patricola and Wehner (2018) found that the response of tropical cyclone precipitation to future warming does not vary for a range of resolutions going from 25 to 2 km. Their results, together with those presented in this study, suggest that the large-scale moisture balance of TC plays an important role in setting TCP in convection permitting models too. Recent experiments carried out in the project DYAMOND (Dynamics of the Atmospheric General Circulation Modeled on Nonhydrostatic Domains; Stevens et al. 2019) will be used in future work to investigate this question.

The large-scale balance of the moisture budget of TCs, as revealed in this study, is particularly interesting to understand the response of TCP to future forcing in GCMs. If future changes of the large-scale environment, and low-level tropospheric humidity in particular, are not impacted by resolution, then we would expect low- and high-resolution models to simulate similar precipitation changes.

Acknowledgments. This work has been funded by the European Union's Horizon 2020 programme under Grant Agreement 641727. We thank three anonymous reviewers for their constructive remarks and suggestions. We thank Kevin Reed, Helen Dacre, Chris Holloway, Nick Klingaman, Jianfeng Gu, and Ralf Toumi for fruitful discussions and suggestions.

REFERENCES

Arakawa, A., 2004: The cumulus parameterization problem: Past, present, and future. *J. Climate*, **17**, 2493–2525, https://doi.org/10.1175/1520-0442(2004)017<2493:RATCPP>2.0.CO;2.

Bacmeister, J. T., M. F. Wehner, R. B. Neale, A. Gettelman, C. Hannay, P. H. Lauritzen, J. M. Caron, and J. E. Truesdale, 2014: Exploratory high-resolution climate simulations using the Community Atmosphere Model (CAM). *J. Climate*, **27**, 3073–3099, https://doi.org/10.1175/JCLI-D-13-00387.1.

——, K. A. Reed, C. Hannay, P. Lawrence, S. Bates, J. E. Truesdale, N. Rosenbloom, and M. Levy, 2016: Projected changes in tropical cyclone activity under future warming scenarios using a high-resolution climate model. *Climatic Change*, **146**, 547–560, https://doi.org/10.1007/s10584-016-1750-x.

Bador, M., and Coauthors, 2020: Impact of higher spatial atmospheric resolution on precipitation extremes over land in global climate models. *J. Geophys. Res. Atmos.*, **125**, e2019JD032184, https://doi.org/10.1029/2019JD032184.

Bechtold, P., E. Bazile, F. Guichard, P. Mascart, and E. Richard, 2001: A mass-flux convection scheme for regional and global models. *Quart. J. Roy. Meteor. Soc.*, **127**, 869–886, https://doi.org/10.1002/qj.49712757309.

Bougeault, P., 1985: A simple parameterization of the large-scale effects of cumulus convection. *Mon. Wea. Rev.*, **113**, 2108–2121, https://doi.org/10.1175/1520-0493(1985)113<2108:ASPOTL>2.0.CO;2.

Braun, S. A., 2006: High-resolution simulation of Hurricane Bonnie (1998). Part II: Water budget. *J. Atmos. Sci.*, **63**, 43–64, https://doi.org/10.1175/JAS3609.1.

Caron, L.-P., C. G. Jones, and K. Winger, 2011: Impact of resolution and downscaling technique in simulating recent Atlantic tropical cyclone activity. *Climate Dyn.*, **37**, 869–892, https://doi.org/10.1007/s00382-010-0846-7.

Chavas, D. R., and J. Vigh, 2014: QSCAT-R: The QuikSCAT tropical cyclone radial structure dataset. NCAR Tech. Note NCAR/TN-5131STR, 25 pp., https://doi.org/10.5065/D6J67DZ4.

Cherchi, A., and Coauthors, 2019: Global mean climate and main patterns of variability in the CMCC-CM2 coupled model. *J. Adv. Model. Earth Syst.*, **11**, 185–209, https://doi.org/10.1029/2018MS001369.

Copernicus Climate Change Service, 2017: ERA5: Fifth generation of ECMWF atmospheric reanalyses of the global climate. ECMWF Tech. Rep., 27 pp.

Dacre, H. F., P. A. Clark, O. Martinez-Alvarado, M. A. Stringer, and D. A. Lavers, 2015: How do atmospheric rivers form? *Bull. Amer. Meteor. Soc.*, **96**, 1243–1255, https://doi.org/10.1175/BAMS-D-14-00031.1.

Dagan, G., P. Stier, and D. Watson-Parris, 2019: Analysis of the atmospheric water budget for elucidating the spatial scale of precipitation changes under climate change. *Geophys. Res. Lett.*, **46**, 10 504–10 511, https://doi.org/10.1029/2019GL084173.

Dee, D. P., and Coauthors, 2011: The ERA-Interim reanalysis: Configuration and performance of the data assimilation system. *Quart. J. Roy. Meteor. Soc.*, **137**, 553–597, https://doi.org/10.1002/qj.828.

Downloaded from http://journals.ametsoc.org/jcli/article-pdf/33/19/8457/4995419/jcli190099.pdf by guest on 16 September 2020

Emanuel, K. A., 1986: An air–sea interaction theory for tropical cyclones. Part I: Steady-state maintenance. *J. Atmos. Sci.*, **43**, 585–605, https://doi.org/10.1175/1520-0469(1986)043<0585:AASITF>2.0.CO;2.

——, 2018: 100 years of progress in tropical cyclone research. *A Century of Progress in Atmospheric and Related Sciences: Celebrating the American Meteorological Society Centennial*, *Meteor. Monogr.*, No. 59, Amer. Meteor. Soc., https://doi.org/10.1175/AMSMONOGRAPHS-D-18-0016.1.

Gelaro, R., and Coauthors, 2017: The Modern-Era Retrospective Analysis for Research and Applications, version 2 (MERRA-2). *J. Climate*, **30**, 5419–5454, https://doi.org/10.1175/JCLI-D-16-0758.1.

Gentry, M. S., and G. M. Lackmann, 2010: Sensitivity of simulated tropical cyclone structure and intensity to horizontal resolution. *Mon. Wea. Rev.*, **138**, 688–704, https://doi.org/10.1175/2009MWR2976.1.

Gregory, D., and P. Rowntree, 1990: A mass flux convection scheme with representation of cloud ensemble characteristics and stability-dependent closure. *Mon. Wea. Rev.*, **118**, 1483–1506, https://doi.org/10.1175/1520-0493(1990)118<1483:AMFCSW>2.0.CO;2.

Guo, L., N. P. Klingaman, P. L. Vidale, A. G. Turner, M.-E. Demory, and A. Cobb, 2017: Contribution of tropical cyclones to atmospheric moisture transport and rainfall over East Asia. *J. Climate*, **30**, 3853–3865, https://doi.org/10.1175/JCLI-D-16-0308.1.

Haarsma, R., and Coauthors, 2020: HighResMIP versions of EC-Earth: EC-Earth3P and EC-Earth3P-HR: Description, model performance, data handling and validation. *Geosci. Model Dev. Discuss.*, https://doi.org/10.5194/gmd-2019-350.

Hodges, K., A. Cobb, and P. L. Vidale, 2017: How well are tropical cyclones represented in reanalysis datasets? *J. Climate*, **30**, 5243–5264, https://doi.org/10.1175/JCLI-D-16-0557.1.

Huffman, G. J., and Coauthors, 2007: The TRMM Multisatellite Precipitation Analysis (TMPA): Quasi-global, multiyear, combined-sensor precipitation estimates at fine scales. *J. Hydrometeor.*, **8**, 38–55, https://doi.org/10.1175/JHM560.1.

Jakob, C., M. Singh, and L. Jungandreas, 2019: Radiative convective equilibrium and organized convection: An observational perspective. *J. Geophys. Res. Atmos.*, **124**, 5418–5430, https://doi.org/10.1029/2018JD030092.

Janssen, P., and J.-R. Bidlot, 2018: Progress in operational wave forecasting. *Procedia IUTAM*, **26**, 14–29, https://doi.org/10.1016/j.piutam.2018.03.003.

Jiang, H., and E. J. Zipser, 2010: Contribution of tropical cyclones to the global precipitation from eight seasons of TRMM data: Regional, seasonal, and interannual variations. *J. Climate*, **23**, 1526–1543, https://doi.org/10.1175/2009JCLI3303.1.

Joyce, R. J., J. E. Janowiak, P. A. Arkin, and P. Xie, 2004: CMORPH: A method that produces global precipitation estimates from passive microwave and infrared data at high spatial and temporal resolution. *J. Hydrometeor.*, **5**, 487–503, https://doi.org/10.1175/1525-7541(2004)005<0487:CAMTPG>2.0.CO;2.

Kim, D., and Coauthors, 2018: Process-oriented diagnosis of tropical cyclones in high-resolution GCMs. *J. Climate*, **31**, 1685–1702, https://doi.org/10.1175/JCLI-D-17-0269.1.

Klaver, R., R. Haarsma, P. L. Vidale, and W. Hazeleger, 2020: Effective resolution in high resolution global atmospheric models for climate studies. *Atmos. Sci. Lett.*, **21**, e952, https://doi.org/10.1002/asl.952.

Knapp, K. R., M. C. Kruk, D. H. Levinson, H. J. Diamond, and C. J. Neumann, 2010: The International Best Track Archive for Climate Stewardship (IBTrACS): Unifying tropical cyclone data. *Bull. Amer. Meteor. Soc.*, **91**, 363–376, https://doi.org/10.1175/2009BAMS2755.1.

Knutson, T. R., and R. E. Tuleya, 2004: Impact of CO_2-induced warming on simulated hurricane intensity and precipitation: Sensitivity to the choice of climate model and convective parameterization. *J. Climate*, **17**, 3477–3495, https://doi.org/10.1175/1520-0442(2004)017<3477:IOCWOS>2.0.CO;2.

——, and Coauthors, 2010: Tropical cyclones and climate change. *Nat. Geosci.*, **3**, 157–163, https://doi.org/10.1038/ngeo779.

Kobayashi, S., and Coauthors, 2015: The JRA-55 Reanalysis: General specifications and basic characteristics. *J. Meteor. Soc. Japan*, **93**, 5–48, https://doi.org/10.2151/jmsj.2015-001.

Magnusson, L., and Coauthors, 2019: ECMWF activities for improved hurricane forecasts. *Bull. Amer. Meteor. Soc.*, **100**, 445–458, https://doi.org/10.1175/BAMS-D-18-0044.1.

Malkus, J. S., and H. Riehl, 1960: On the dynamics and energy transformations in steady-state hurricanes. *Tellus*, **12** (1), 1–20, https://doi.org/10.3402/tellusa.v12i1.9351.

Manganello, J. V., and Coauthors, 2012: Tropical cyclone climatology in a 10-km global atmospheric GCM: Toward weather-resolving climate modeling. *J. Climate*, **25**, 3867–3893, https://doi.org/10.1175/JCLI-D-11-00346.1.

Montgomery, M. T., M. E. Nicholls, T. A. Cram, and A. B. Saunders, 2006: A vortical hot tower route to tropical cyclogenesis. *J. Atmos. Sci.*, **63**, 355–386, https://doi.org/10.1175/JAS3604.1.

Moon, Y., and Coauthors, 2020: Azimuthally averaged wind and thermodynamic structures of tropical cyclones in global climate models and their sensitivity to horizontal resolution. *J. Climate*, **33**, 1575–1595, https://doi.org/10.1175/JCLI-D-19-0172.1.

Neale, R. B., and Coauthors, 2010: Description of the NCAR Community Atmosphere Model (CAM5.0). NCAR Tech. Note NCAR/TN-486+STR, 268 pp., www.cesm.ucar.edu/models/cesm1.1/cam/docs/description/cam5_desc.pdf.

Ooyama, K. V., 1982: Conceptual evolution of the theory and modeling of the tropical cyclone. *J. Meteor. Soc. Japan*, **60**, 369–380, https://doi.org/10.2151/jmsj1965.60.1_369.

Patricola, C. M., and M. F. Wehner, 2018: Anthropogenic influences on major tropical cyclone events. *Nature*, **563**, 339–346, https://doi.org/10.1038/s41586-018-0673-2.

Reed, K. A., and C. Jablonowski, 2011: Impact of physical parameterizations on idealized tropical cyclones in the Community Atmosphere Model. *Geophys. Res. Lett.*, **38**, L04805, https://doi.org/10.1029/2010GL046297.

Roberts, C. D., R. Senan, F. Molteni, S. Boussetta, M. Mayer, and S. P. E. Keeley, 2018: Climate model configurations of the ECMWF Integrated Forecasting System (ECMWF-IFS cycle 43r1) for HighResMIP. *Geosci. Model Dev.*, **11**, 3681–3712, https://doi.org/10.5194/gmd-11-3681-2018.

Roberts, M. J., and Coauthors, 2015: Tropical cyclones in the UPSCALE ensemble of high-resolution global climate models. *J. Climate*, **28**, 574–596, https://doi.org/10.1175/JCLI-D-14-00131.1.

——, and Coauthors, 2018: The benefits of global high resolution for climate simulation: Process understanding and the enabling of stakeholder decisions at the regional scale. *Bull. Amer. Meteor. Soc.*, **99**, 2341–2359, https://doi.org/10.1175/BAMS-D-15-00320.1.

——, and Coauthors, 2020: Impact of model resolution on tropical cyclone simulation using the HighResMIP–PRIMAVERA multimodel ensemble. *J. Climate*, **33**, 2557–2583, https://doi.org/10.1175/JCLI-D-19-0639.1.

Scoccimarro, E., S. Gualdi, G. Villarini, G. A. Vecchi, M. Zhao, K. Walsh, and A. Navarra, 2014: Intense precipitation events associated with landfalling tropical cyclones in response to a

Downloaded from http://journals.ametsoc.org/jcli/article-pdf/33/19/8457/4995419/jcli190099.pdf by guest on 16 September 2020

warmer climate and increased CO_2. *J. Climate*, **27**, 4642–4654, https://doi.org/10.1175/JCLI-D-14-00065.1.

——, ——, A. Bellucci, D. Peano, A. Cherchi, G. A. Vecchi, and A. Navarra, 2020: The typhoon-induced drying of the Maritime Continent. *Proc. Natl. Acad. Sci. USA*, **117**, 3983–3988, https://doi.org/10.1073/pnas.1915364117.

Shaevitz, D. A., and Coauthors, 2014: Characteristics of tropical cyclones in high-resolution models in the present climate. *J. Adv. Model. Earth Syst.*, **6**, 1154–1172, https://doi.org/10.1002/2014MS000372.

Simpson, J., E. Ritchie, G. Holland, J. Halverson, and S. Stewart, 1997: Mesoscale interactions in tropical cyclone genesis. *Mon. Wea. Rev.*, **125**, 2643–2661, https://doi.org/10.1175/1520-0493(1997)125<2643:MIITCG>2.0.CO;2.

Skok, G., J. Bacmeister, and J. Tribbia, 2013: Analysis of tropical cyclone precipitation using an object-based algorithm. *J. Climate*, **26**, 2563–2579, https://doi.org/10.1175/JCLI-D-12-00135.1.

Smith, R. K., 2000: The role of cumulus convection in hurricanes and its representation in hurricane models. *Rev. Geophys.*, **38**, 465–489, https://doi.org/10.1029/1999RG000080.

Stevens, B., and Coauthors, 2019: DYAMOND: The dynamics of the atmospheric general circulation modeled on non-hydrostatic domains. *Prog. Earth Planet. Sci.*, **6**, 61, https://doi.org/10.1186/s40645-019-0304-z.

Strachan, J., P. L. Vidale, K. Hodges, M. Roberts, and M.-E. Demory, 2013: Investigating global tropical cyclone activity with a hierarchy of AGCMs: The role of model resolution. *J. Climate*, **26**, 133–152, https://doi.org/10.1175/JCLI-D-12-00012.1.

Trenberth, K. E., C. A. Davis, and J. Fasullo, 2007: Water and energy budgets of hurricanes: Case studies of Ivan and Katrina. *J. Geophys. Res.*, **112**, D23106, https://doi.org/10.1029/2006JD008303.

Villarini, G., and G. A. Vecchi, 2012: Twenty-first-century projections of North Atlantic tropical storms from CMIP5 models. *Nat. Climate Change*, **2**, 604–607, https://doi.org/10.1038/nclimate1530.

Vincent, E. M., M. Lengaigne, G. Madec, J. Vialard, G. Samson, N. C. Jourdain, C. E. Menkes, and S. Jullien, 2012a: Processes setting the characteristics of sea surface cooling induced by tropical cyclones. *J. Geophys. Res.*, **117**, C02020, https://doi.org/10.1029/2011JC007396.

——, ——, J. Vialard, G. Madec, N. C. Jourdain, and S. Masson, 2012b: Assessing the oceanic control on the amplitude of sea surface cooling induced by tropical cyclones. *J. Geophys. Res.*, **117**, C05023, https://doi.org/10.1029/2011JC007705.

Voldoire, A., and Coauthors, 2019: Evaluation of CMIP6 DECK experiments with CNRM-CM6-1. *J. Adv. Model. Earth Syst.*, **11**, 2177–2213, https://doi.org/10.1029/2019MS001683.

Wing, A. A., and Coauthors, 2019: Moist static energy budget analysis of tropical cyclone intensification in high-resolution climate models. *J. Climate*, **32**, 6071–6095, https://doi.org/10.1175/JCLI-D-18-0599.1.

Zhao, M., I. M. Held, and S.-J. Lin, 2012: Some counterintuitive dependencies of tropical cyclone frequency on parameters in a GCM. *J. Atmos. Sci.*, **69**, 2272–2283, https://doi.org/10.1175/JAS-D-11-0238.1.

Zhou, W., I. M. Held, and S. T. Garner, 2014: Parameter study of tropical cyclones in rotating radiative–convective equilibrium with column physics and resolution of a 25-km GCM. *J. Atmos. Sci.*, **71**, 1058–1069, https://doi.org/10.1175/JAS-D-13-0190.1.

——, ——, and ——, 2017: Tropical cyclones in rotating radiative–convective equilibrium with coupled SST. *J. Atmos. Sci.*, **74**, 879–892, https://doi.org/10.1175/JAS-D-16-0195.1.

Downloaded from http://journals.ametsoc.org/jcli/article-pdf/33/19/8457/4995419/jcli190099.pdf by guest on 16 September 2020